Cerebral Cortex August 2015;25:2114–2126
doi:10.1093/cercor/bhu020
Advance Access publication February 18, 2014

Canonical Organization of Layer 1 Neuron-Led Cortical Inhibitory and Disinhibitory Interneuronal Circuits

Alice J. Lee[1,3], Guangfu Wang[1], Xiaolong Jiang[1], Seraphina M. Johnson[1,4], Elizabeth T. Hoang[1,5], Fabien Lanté[1], Ruth L. Stornetta[1], Mark P. Beenhakker[1], Ying Shen[6] and J. Julius Zhu[1,2]

[1]Department of Pharmacology, [2]Department of Neuroscience, [3]Department of Biology, [4]Department of Chemistry, [5]Department of Psychology, School of Medicine and College of Arts and Sciences, University of Virginia, Charlottesville, VA 22908, USA and [6]Department of Neurobiology and Key Laboratory of Medical Neurobiology of Chinese Ministry of Health, Zhejiang University School of Medicine, 388 Yu Hang Tang Road, Hangzhou 310058, PR China

Alice J. Lee, Guangfu Wang, and Xiaolong Jiang authors contributed equally.

Address correspondence to J. Julius Zhu, Department of Pharmacology, University of Virginia School of Medicine, 1300 Jefferson Park Avenue, Charlottesville, VA 22908, USA. Email: jjzhu@virginia.edu

Interneurons play a key role in cortical function and dysfunction, yet organization of cortical interneuronal circuitry remains poorly understood. Cortical Layer 1 (L1) contains 2 general GABAergic interneuron groups, namely single bouquet cells (SBCs) and elongated neurogliaform cells (ENGCs). SBCs predominantly make unidirectional inhibitory connections (SBC→) with L2/3 interneurons, whereas ENGCs frequently form reciprocal inhibitory and electric connections (ENGC↔) with L2/3 interneurons. Here, we describe a systematic investigation of the pyramidal neuron targets of L1 neuron-led interneuronal circuits in the rat barrel cortex with simultaneous octuple whole-cell recordings and report a simple organizational scheme of the interneuronal circuits. Both SBCs→ and ENGC ↔ L2/3 interneuronal circuits connect to L2/3 and L5, but not L6, pyramidal neurons. SBC → L2/3 interneuronal circuits primarily inhibit the entire dendritic–somato–axonal axis of a few L2/3 and L5 pyramidal neurons located within the same column. In contrast, ENGC ↔ L2/3 interneuronal circuits generally inhibit the distal apical dendrite of many L2/3 and L5 pyramidal neurons across multiple columns. Finally, L1 interneuron-led circuits target distinct subcellular compartments of L2/3 and L5 pyramidal neurons in a L2/3 interneuron type-dependent manner. These results suggest that L1 neurons form canonical interneuronal circuits to control information processes in both supra- and infragranular cortical layers.

Keywords: attention, circuits, cortex, disinhibition, inhibition, interneurons, salient selection

Introduction

The cerebral cortex is a remarkable structure composed of extensive replications of smaller modules, and embedded within these modules are excitatory cortical neurons that form "canonical" neuronal circuits with similar design and operation (Gilbert and Wiesel 1983; Mountcastle 1997; Douglas and Martin 2007; Petersen 2007; Nassi and Callaway 2009; Meyer et al. 2010). It remains uncertain whether canonical organization principles apply to construction of cortical inhibitory neuronal circuits. The lag of understanding interneuronal circuits is largely due to the technical difficulty of systematically decoding connection diagrams among identified interneurons and their targets. Nevertheless, recent analysis has revealed that cortical interneurons receive inputs and dispatch outputs following a few standard patterns (Xu and Callaway 2009; Katzel et al. 2011; Pfeffer et al. 2013), supporting the hypothesis that cortical interneurons may also form canonical neuronal circuits.

We recently reported that L1 single bouquet cells (SBCs) predominantly make unidirectional inhibitory connections (→) with all seven types of L2/3 interneurons (SBC → L2/3 interneuronal circuits), whereas L1 elongated neurogliaform cells (ENGCs) frequently form reciprocal inhibitory and electric connections (↔) with 3 types of L2/3 interneurons (ENGC ↔ L2/3 interneuronal circuits) (Jiang et al. 2013). To decipher the general organization scheme of cortical interneuronal circuits, we systematically analyzed the pyramidal neuron targets of 2 Layer 1 (L1) interneuron-led circuits in acute rat barrel cortical slices, using a recently developed stable octuple whole-cell recording technology (Jiang et al. 2013). We found that both SBC → L2/3 and ENGC ↔ L2/3 interneuronal circuits innervated pyramidal neurons in L2/3 and L5, but not L6. SBC → L2/3 interneuronal circuits formed synapses on both the apical and oblique/basal dendritic domains of a small number of L2, L3, L5a and L5b pyramidal neurons located within the same column. In contrast, ENGC ↔ L2/3 interneuronal circuits formed synapses on the apical dendritic domain of a large population of L2, L3, L5a and 5b pyramidal neurons across multiple columns. Finally, SBC → L2/3 and ENGC ↔ L2/3 interneuronal circuits target distinct subcellular dendritic–somato–axonal compartments of L2, L3, L5a and 5b pyramidal neurons in a L2/3 interneuron type-dependent manner. These results suggest that cortical L1 interneurons lead canonical interneuronal circuits that target pyramidal neurons in both supra- and infragranular layers.

Materials and Methods

Animal Preparation

Young and adult male and female Sprague Dawley rats (≥postnatal p20–42; $n = 1104$), whose cortical inhibitory neurons and circuits are largely mature and relatively stabilized (Huang et al. 2007; Batista-Brito and Fishell 2009), were used for in vitro experiments in this study. All procedures for animal surgery and maintenance were performed following protocols approved by the Animal Care & Use Committee of the University of Virginia (Protocol No. 3168) and in accordance with US National Institutes of Health guidelines. The cortical brain slice preparation followed our previous studies (Zhu 2000; Larkum and Zhu 2002). In brief, animals were deeply anesthetized by sodium pentobarbital (90 mg/kg) and decapitated. The brain was quickly removed and placed into cold (0–4°C) oxygenated physiological solution containing (in mM): 125 NaCl, 2.5 KCl, 1.25 NaH_2PO_4, 25 $NaHCO_3$, 1 $MgCl_2$, 25 dextrose, and 2 $CaCl_2$ (pH 7.4). Parasagittal slices 350 μm thick were cut from the tissue blocks with a microslicer, at an angle (<~4°) closely parallel to apical dendrites of L5 pyramidal neurons, which retained

the majority of distal ascending and descending axonal trees of L1–3 interneurons that project into L1 and L5–6. These slices were kept at 37.0 ± 0.5°C in oxygenated physiological solution for ~0.5–1 h before recordings. During the recording, the slices were submerged in a chamber and stabilized with a fine nylon net attached to a platinum ring. The recording chamber was perfused with oxygenated physiological solution containing additional AMPA- and NMDA-receptor antagonists 20 μM DNQX and 100 μM DL-APV. The half-time for the bath solution exchange was ~6 s, and the temperature of the bath solution was maintained at 34.0 ± 0.5°C. All antagonists were bath applied.

Histology and Electron Microscopy

Light and electron microscopic (LM and EM) examinations were carried out following the procedures of our previous reports (Larkum and Zhu 2002; Kielland et al. 2009; Jiang et al. 2013). In brief, after in vitro recordings, the slices were fixed by immersion in 3% acrolein/4% paraformaldehyde in 0.1 M PBS at 4°C for 24 h, and then processed with the avidin–biotin–peroxidase method to reveal cell morphology. Some of the slices were subsequently sectioned into 60 μm sections, postfixed in 1% OsO_4, counterstained with 1% uranyl acetate, and flat embedded into resin to carry out EM examination. The morphologically recovered cells were examined, drawn, and analyzed with the aid of a microscope equipped with a ×100 oil immersion objective and a computerized reconstruction system Neurolucida (MicroBrightField, Colchester, VT, USA). L2, L3, L5a and L5b pyramidal neurons were normalized according to the soma and their apical dendrites, with the length of their apical dendrites set arbitrarily as 300, 500, 900 and 1100 μm, respectively (cf. (Larkum and Zhu 2002; Jiang et al. 2013)). For EM examination, the small areas of interest (~50 μm × ~50 μm), each containing putative synaptic boutons from single presynaptic neurons, were embedded in resin, carefully excised and resectioned into 80 nm serial ultrathin sections using an ultramicrotome. No excision and resection was made if synaptic boutons originated from different presynaptic neurons that were too close to be separated. The serial ultrathin sections were examined in sequence with a JEOL-1230 transmission electron microscope (Japan Electron Optic, Tokyo, Japan) following the labeled dendrites, which typically led to all LM-identified synapses (except a very few synapses destroyed during EM processing or hidden behind the grids) at the order predicted by Neurolucida reconstruction. Inhibitory synaptic contacts were determined based on generally accepted criteria, including (i) presence of membranes with parallel alignment forming synaptic clefts that are wider in the middle and close up at one or both edges, (ii) absence of a prominent postsynaptic density, and (iii) presence of multiple flattened synaptic vesicles with at least one docked at the presynaptic membrane.

Electrophysiology

Simultaneous whole-cell in vitro recordings were obtained from neurons in the barrel cortex as described previously (Larkum and Zhu 2002; Zhu 2009; Jiang et al. 2013). Briefly, patch recording pipettes (4–7 MΩ) were filled with intracellular solutions containing (mM): 135 cesium methanesulfonate, 10 HEPES, 2.5 $MgCl_2$, 4 Na_2ATP, 0.4 Na_3GTP, 10 sodium phosphocreatine, 0.6 EGTA, 0.1 spermine and 0.5% biocytin, at pH 7.25 for current recordings, or 120 potassium gluconate, 10 HEPES, 4 KCl, 4 MgATP, 0.3 Na_3GTP, 10 sodium phosphocreatine, and 0.5% biocytin, at pH 7.25, for voltage recordings. Whole-cell recordings were made with up to eight Axopatch 200B and/or Axoclamp 2A/B amplifiers (Molecular Devices, Sunnyvale, CA, USA). SBCs preferentially inhibit L2/3 interneurons located within narrow perpendicular columns below their somata and ENGCs preferentially inhibit L2/3 interneurons located within the upper L2/3 (Supplementary Fig. 1 and Tables 1 and 2; see also Jiang et al. 2013). Therefore, to increase the success rate of finding L2/3 interneurons innervated by L1 interneurons, we targeted recordings of L2/3 interneurons in these specific regions after defining the putative identity of L1 interneurons based on their firing patterns. L2–6 pyramidal neurons located in both the same and neighboring columns relative to L1 interneurons were randomly sampled after L1–2/3 interneuronal connections were established. The column borders were determined by referring to the barrels, typically ~230 ± 50 μm in diameter (Agmon and Connors 1991), as well as the characteristic clusters of ~10–20 closely packed large L5 pyramidal neurons located just inside of the columnar borders (Ito 1992; Zhu 2000). An ITC-18 interface board (HEKA Instruments Inc, Bellmore, NY, USA) was custom-modified to achieve simultaneous A/D and D/A conversions of current, voltage, command, and triggering signal for up to 8 amplifiers. Custom-written Igor-based programs were used to operate the recording system and perform online and offline data analysis. Motorized manipulators (Lugis & Neumann Feinmechanik and Elektrotechnik, Ratingen, Germany) were custom improved in stability to improve morphological recovery of axonal arborization of the recorded interneurons. More than 85% of recorded interneurons had their axonal arborization well recovered and thus could be unambiguously classified into anatomical groups. These interneurons were included in the analysis. The L2/3 border was determined somewhat arbitrarily at approximately the halfway between the top of L2 and the bottom of L3 considering L2 having the more granular appearance and higher packing density of neurons (Brecht et al. 2003; Shepherd and Svoboda 2005). The L5a/b border was marked by a gradual increase in cell density and the appearance of larger neurons (Manns et al. 2004). We could anatomically locate 533 pyramidal neurons reported in our previous study (Jiang et al. 2013) into either L5a or L5b of the barrel cortex. Thus, these neurons were reanalyzed and included in this study. The L5b/L6 border was indicated by a relatively cell free stripe between large L5b neurons and smaller layer 6 neurons with shorter apical dendrites (Zhang and Deschenes 1997; Manns et al. 2004). Based on the previously developed criteria (Zhang and Deschenes 1997), L6 pyramidal neurons, with their apical dendrites projecting to middle layers and axons collaterals running primarily upward and vertically within a column, were defined as tentative corticothalamic neurons. In contrast, L6 short, inverted or modified pyramidal neurons, or spiny bipolar neurons, with their axons running more horizontally in the infragranular layers and white matter, were named as putative corticocortical neurons. The presynaptic single action potential-evoked uIPSCs or uIPSPs in >3-week-old cortical neurons are highly reliable and often show no transmission failure (Tamas et al. 2002; Szabadics et al. 2007). Thus, inhibitory synaptic connections could be unambiguously

Table 1
Comparison of the depth of L2/3 interneurons innervated by SBCs and ENGCs

Postsynaptic interneurons	L2/3l innervated by SBCs (μm)	L2/3l innervated by ENGCs (μm)	*U* and *P* value (M–W rank sum)	
MaC	383 ± 44 (n = 11)	247 ± 17 (n = 14)	32.0	0.015
NGC	317 ± 18 (n = 22)	213 ± 10 (n = 29)	132.5	<0.001
BTC	322 ± 20 (n = 30)	212 ± 12 (n = 22)	551.0	<0.001
BPC	367 ± 29 (n = 21)	—	—	—
BaC	327 ± 26 (n = 26)	—	—	—
DBC	355 ± 22 (n = 22)	—	—	—
ChC	283 ± 34 (n = 13)	—	—	—

Note: No significant difference in the depth among seven different interneuron group innervated by SBCs or 3 different interneurons innervated by ENGCs ($P > 0.05$; Mann–Whitney rank-sum tests).

Table 2
Comparison of the relative lateral distance of L2/3 interneurons to their presynaptic SBCs and ENGCs

Postsynaptic interneurons	L2/3l innervated by SBCs (μm)	L2/3l innervated by ENGCs (μm)	*U* and *P* value (M–W rank sum)	
MaC	16 ± 3 (n = 11)	50 ± 12 (n = 14)	107.0	0.106
NGC	16 ± 3 (n = 22)	41 ± 6 (n = 29)	488.0	0.001
BTC	17 ± 2 (n = 30)	44 ± 9 (n = 22)	194.5	0.012
BPC	17 ± 3 (n = 21)	—	—	—
BaC	17 ± 3 (n = 26)	—	—	—
DBC	17 ± 3 (n = 22)	—	—	—
ChC	17 ± 4 (n = 13)	—	—	—

Note: No significant difference in the relative lateral distance to their presynaptic L1 interneurons among seven different interneuron group innervated by SBCs or 3 different interneurons innervated by ENGCs ($P > 0.05$; Mann–Whitney rank-sum tests).

identified after online monitoring of the average responses of short latency uIPSPs for ≥50 episodes. Unless otherwise specified, IPSCs and IPSPs were measured with membrane potentials of postsynaptic cells clamped or held at −55 and −55 ± 3 mV, respectively. Recording traces shown were typically averages of 50–200 consecutive episodes.

Statistical Analysis

Statistical results were reported as mean ± SEM unless stated otherwise. The sample size (n) represents the number of neurons, unless otherwise indicated. Statistical significances of the means ($P \leq 0.05$; 2 sides) were determined using Mann–Whitney rank-sum and χ^2-tests.

Results

We analyzed the synaptic connections among 4587 L1–3 interneurons and 6519 L2–6 pyramidal neurons in brain slices acutely prepared from the rat barrel cortex. Inhibitory synaptic connections were identified by evoking unitary inhibitory postsynaptic currents (uIPSCs) or potentials (uIPSPs) with brief depolarizing current pulses (5 ms) applied in presynaptic neurons at 0.01–0.05 Hz in the presence of AMPA- and NMDA-receptor antagonists (20 μM DNQX and 100 μM DL-APV). Based on previously established axonal arborization-based interneuronal classification schemes (Markram et al. 2004; Ascoli et al. 2008; Jiang et al. 2013; Kubota 2014), we could unambiguously classify L1–3 interneurons into 9 general groups, including SBCs ($n = 581$), ENGCs ($n = 268$) in L1, Martinotti cells (MaCs, $n = 361$), neurogliaform cells (NGCs, $n = 752$), bitufted cells (BTCs, $n = 1{,}402$), bipolar cells (BPCs, $n = 187$), basket cells (BaCs, $n = 608$), double-bouquet cells (DBCs, $n = 243$), and chandelier cells (ChCs, $n = 185$) in L2/3.

Laminar Organization of L1 Interneuronal Circuits

We first recorded L1 interneurons, and then made targeted recordings from L2/3 interneurons potentially innervated by L1 interneurons (see Materials and Methods). After establishing synaptic connections between L1 and L2/3 interneurons, we further searched postsynaptic pyramidal neurons targeted by SBC→ and ENGC ↔ L2/3 interneuronal circuits in L2–6 (Figs 1 and 2). We found that both SBC- and ENGC-led interneuronal circuits formed inhibitory synapses on pyramidal neurons in L2/3 and L5, but not L6 (Figs 1 and 2 and Tables 3–6).

Within the same columns, single SBCs made occasional connections with L2/3 (~0.5%) and L5 (~0.2%) pyramidal neurons, but no connections with L6 pyramidal neurons (Fig. 1*C* and Tables 7 and 8). In contrast, single L2/3 interneurons innervated by SBCs inhibited ~35% of L2 and L3 pyramidal neurons in a L2/3 interneuron cell type-dependent manner, ranging from ~8% for BPCs to ~70% for NGCs (Fig. 1*C* and Table 7). In addition, single L2/3 interneurons innervated by SBCs inhibited ~15% of L5a and L5b pyramidal neurons in a similar cell type-dependent pattern, ranging from ~3% for BPCs to ~30% for NGCs (Fig. 1*C* and Table 8). These L2/3 interneurons inhibited neither L6 corticocortical (CC) nor L6 corticothalamic (CT) pyramidal neurons (Fig. 1*C* and Tables 3 and 4). While SBCs generated only small uIPSPs (~0.05 mV) in L2/3 and L5 pyramidal neurons, L2/3 interneurons in SBC → L2/3 interneuronal circuits produced ~0.25–0.65 mV uIPSPs in L2/3 pyramidal neurons, and ~0.15–0.45 mV uIPSPs in L5 pyramidal neurons (Fig. 1*C* and Tables 9 and 10).

In contrast to SBCs, single ENGCs formed extensive inhibitory connections with L2 and L3 pyramidal neurons (~60%), and frequent with L5a and L5b pyramidal neurons (~20%) within the same columns, but not with L6 CC or CT pyramidal neurons (Fig. 2*C* and Tables 11 and 12). Moreover, single MaCs, NGCs or BTCs innervated by ENGCs inhibited ~25%–55% of L2 and L3 pyramidal neurons, and ~5%–30% of L5a and L5b pyramidal neurons, but none of L6 CC and CT pyramidal neurons (Fig. 2*C* and Tables 3 and 4 and 11 and 12). The average sizes of uIPSPs induced by these 4 types of interneurons in ENGC ↔ L2/3 interneuronal circuits were ~0.40 mV in L2/3 pyramidal neurons and ~0.20 mV in L5 pyramidal neurons (Fig. 2*C* and Tables 13 and 14). Together, these results suggest that SBC→ and ENGC ↔ L2/3 interneuronal circuits control inhibition of pyramidal neurons in L2/3 and L5, but not L6.

Columnar Organization of L1 Interneuronal Circuits

We next investigated how SBC→ and ENGC ↔ L2/3 interneuronal circuits connect to pyramidal neurons in the same and neighboring columns (Figs 3 and 4). Multiple recordings revealed that SBCs inhibited very few intracolumnar L2/3 and L5 pyramidal neurons, but none of the L2/3 and L5 pyramidal neurons in neighboring columns (Fig. 3*C* and Tables 15 and 16). In contrast, single L2/3 interneurons innervated by SBCs inhibited L2 and L3 pyramidal neurons in neighboring columns, although to a much smaller extent (~3%) compared with those in the same columns (Fig. 3*C* and Table 15). Finally, L2/3 interneurons innervated by SBCs only inhibited intracolumnar L5a and L5b pyramidal neurons, but they did not inhibit L5 pyramidal neurons in neighboring columns (Fig. 3*C* and Table 16). Interestingly, many of the pyramidal neurons synaptically connected by SBC → L2/3 interneuronal circuits were located in the close proximity to the vertically projecting axons of SBCs (cf. Jiang et al. 2013). Together, these results suggest that SBC → L2/3 interneuronal circuits preferentially formed inhibitory synapses on L2/3 and L5 pyramidal neurons within the same columns.

In contrast, interneurons in ENGC ↔ L2/3 interneuronal circuits formed inhibitory synapses on L2/3 and L5 pyramidal neurons in both the same and neighboring columns (Fig. 4). Quantitative analysis revealed that single ENGCs inhibited ~25% of L2 pyramidal neurons, ~15% of L3 pyramidal neurons, and ~10% of L5a and L5b pyramidal neurons in neighboring columns, whereas single L2/3 interneurons innervated by ENGCs inhibited ~15% of L2 pyramidal neurons, ~10% of L3 pyramidal neurons in neighboring columns, but none of L5a and L5b pyramidal neurons in neighboring columns (Fig. 4*D* and Tables 17 and 18). Overall, the percentage of pyramidal neurons innervated by ENGC ↔ L2/3 interneuronal circuits in neighboring columns was about half of those in the same columns (Fig. 4*D* and Tables 17 and 18). These results suggest that ENGC ↔ L2/3 interneuronal circuits generally control inhibition of pyramidal neurons across multiple columns.

Synaptic Organization of L1 Interneuronal Circuits

We have previously reported that L1-3 interneurons make synaptic contacts on a largely non-overlapping subcellular compartment of L5 pyramidal neurons, and together they subdivided the entire membrane surface of the dendritic–somato–axonal initial segment region (Jiang et al. 2013). In this study, we compared targeting patterns of inhibitory synapses made by L1–3 interneurons on L2, L3, L5a and L5b pyramidal neurons. In a number of cases ($n = 11$), we made simultaneous recordings from multiple interneurons that inhibited multiple pyramidal neurons

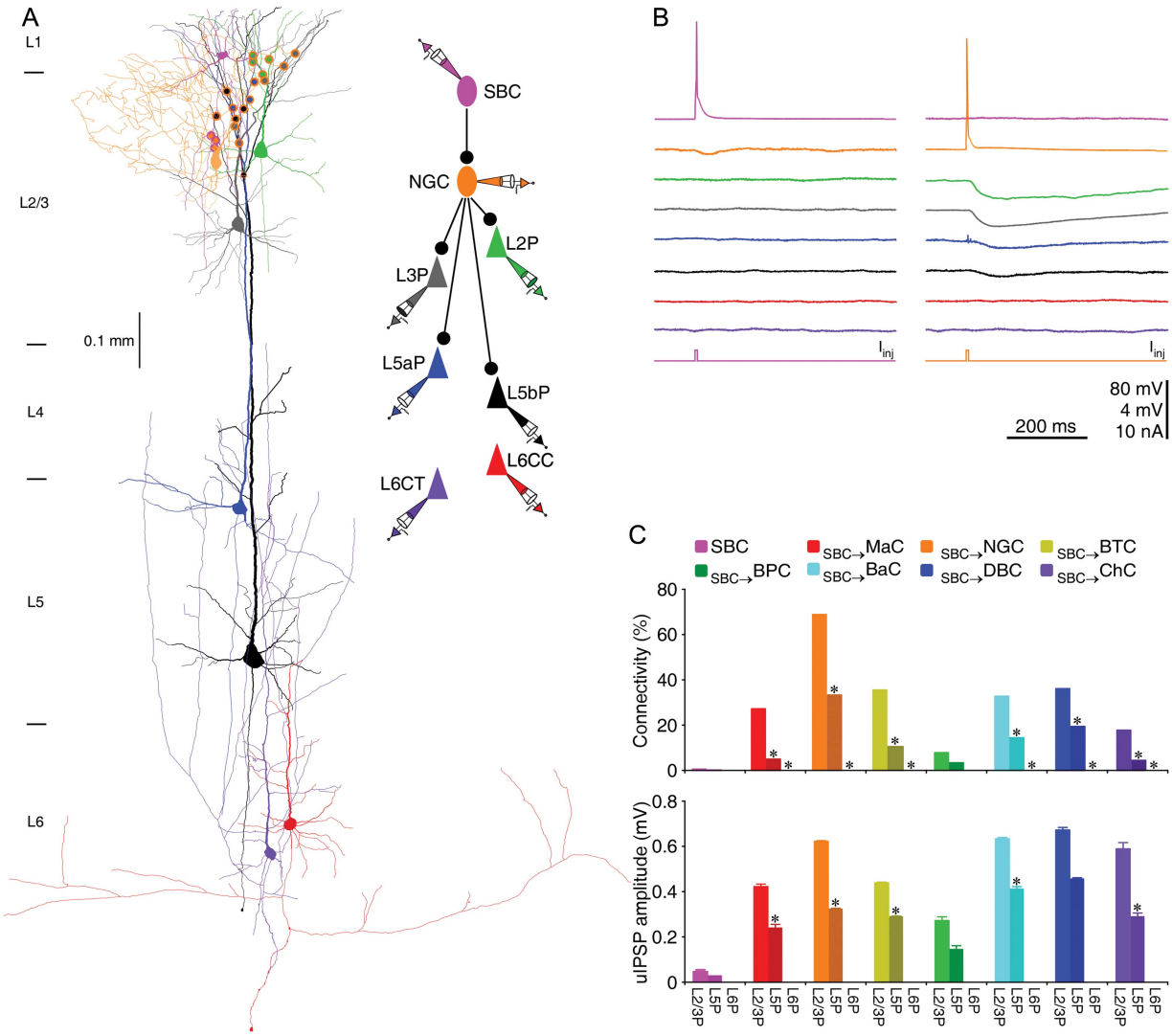

Figure 1. SBC → L2/3 interneuronal circuits disinhibit L2/3 and L5, but not L6 pyramidal neurons. (*A*) Reconstruction of L1 SBC (pink), L2 NGC (brown), and 2 L2/3 (L2P and L3P; green and gray), 2 L5 (L5aP and L5bP; blue and black), 2 L6 (CC or L6CC and CT or L6CT; red and purple) pyramidal neurons recorded simultaneously from an acute cortical slice. The double colored dots indicate the putative synaptic contacts based on anatomical reconstruction. The schematic drawing shows symbolically the synaptic connections. (*B*) Single action potentials elicited in SBC and NGC evoked uIPSPs in postsynaptic NGC, L2/3 and L5 pyramidal neurons, respectively. Scale bars apply to all recording traces with 80 and 4 mV bars applied to traces with and without action potentials, respectively. (*C*) Connectivity and strength of synapses formed by SBC → L2/3 interneuronal circuits on L2–6 pyramidal neurons. Asterisks indicate significant differences ($P < 0.05$) in synaptic connectivity (χ^2-tests) or synaptic strength (Mann–Whitney rank-sum tests) between SBC → L2/3 interneuronal circuits on L2/3 pyramidal neurons and L5 or L6 pyramidal neurons (see Tables 3–6 for values).

located in both L2/3 and L5 (Fig. 5*A*). Postrecording morphological reconstruction showed that specific SBC- and ENGC-innervated L2/3 interneuron subtypes generally targeted similar subcellular compartments of L2/3 and L5 pyramidal neurons. However, the downstream targets of different SBC- and ENGC-innervated L2/3 interneuron subtypes were consistently distinct (Fig. 5 and Supplementary Figs 2 and 3). We found that for L2/3 interneurons innervated by SBCs, the synaptic boutons of MaCs were on terminal tuft dendrites, those of NGCs were on high-order tuft dendrites, those of BTCs were on distal dendritic trunks and primary tuft dendrites, those of BPCs were on middle dendritic trunks and oblique dendrites, those of BaCs were on somata and proximal dendrites, those of DBCs were on middle and distal basal dendrites, and those of ChCs were on axonal initial segments of L2, L3, L5a and L5b pyramidal neurons (Fig. 5*C* and Supplementary Fig. 2 and Tables 19 and 20). Moreover, the synaptic boutons of NGCs innervated by SBCs were also found on distal basal dendrites of L2 and L3 pyramidal neurons but not L5a and L5b pyramidal neurons (Fig. 5*C* and Supplementary Fig. 2 and Tables 19 and 20). Morphological reconstruction further showed that interneurons in ENGC ↔ L2/3 interneuronal circuits formed synapses on the apical dendrites of pyramidal neurons of L2/3 and L5 pyramidal neurons (Supplementary Fig. 3 and Tables 19 and 20). The synaptic boutons of MaCs were on terminal tuft dendrites, those of NGCs were on high-order tuft dendrites, and those of BTCs were on distal dendritic trunks and primary tuft dendrites of L2, L3, L5a and L5b pyramidal neurons (Supplementary Fig. 3 and Tables 19 and 20). Finally, the synaptic boutons of ENGCs were on tuft dendrites of L2, L3, L5a, and L5b pyramidal neurons (Supplementary Fig. 3 and Tables 19 and 20).

To confirm that these synaptic boutons are actual synapses, we carried out ultrastructural analysis of some synaptic boutons after Neurolucida reconstruction. Electron microscopic serial

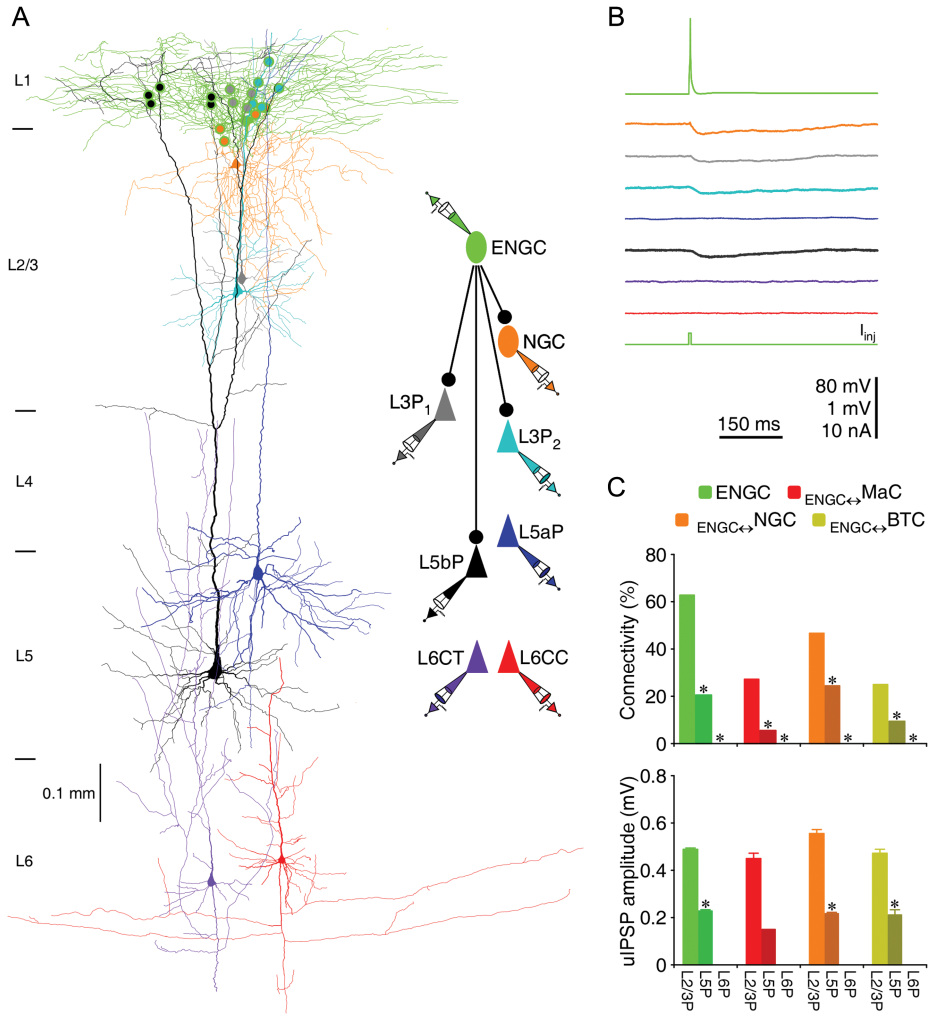

Figure 2. ENGC → L2/3 interneuronal circuits inhibit L2/3 and L5, but not L6 pyramidal neurons. (*A*) Reconstruction of L1 ENGC (green), L2 NGC (brown), and 2 L3 ($L3P_1$ and $L3P_2$; gray and cyan), 2 L5 (L5aP and L5bP; blue and black), 2 L6 (CC or L6CC and CT or L6CT; red and purple) pyramidal neurons recorded simultaneously from an acute cortical slice. The double colored dots indicate the putative synaptic contacts based on anatomical reconstruction. The schematic drawing shows symbolically the synaptic connections. (*B*) Single action potentials elicited in ENGC evoked uIPSPs in postsynaptic NGC, L2/3 and L5 pyramidal neurons. Scale bars apply to all recording traces with 80 and 1 mV bars applied to traces with and without action potentials, respectively. (*C*) Connectivity and strength of synapses formed by ENGC ↔ L2/3 interneuronal circuits on L2–6 pyramidal neurons. Asterisks indicate significant differences ($P < 0.05$) in synaptic connectivity (χ^2-tests) or synaptic strength (Mann–Whitney rank-sum tests) between ENGC ↔ L2/3 interneuronal circuits on L2/3 pyramidal neurons and L5 or L6 pyramidal neurons (see Tables 3–6 for values).

Table 3

Synaptic connectivity between SBC → L2/3I neuronal circuits and L2/3, L5, and L6 pyramidal neurons

Presynaptic interneurons	L2/3 pyramidal neurons (connected/tested and %)		L5 pyramidal neurons (connected/tested and %)		L6 pyramidal neurons (connected/tested and %)	
SBC→	3/565	0.5	1/624	0.2	0/86	0.0
SBC→MaC→	24/88	27.3	8/155	5.9	0/53	0.0
SBC→NGC→	175/254	68.9	157/472	33.3	0/99	0.0
SBC→BTC→	182/512	68.9	116/1,092	33.3	0/162	0.0
SBC→BPC→	8/102	7.8	6/184	3.3	0/37	0.0
SBC→BaC→	105/322	32.6	57/391	14.6	0/115	0.0
SBC→DBC→	53/146	36.3	44/225	19.6	0/81	0.0
SBC→ChC→	13/73	17.8	7/156	4.5	0/141	0.0

Table 4

Synaptic strength between SBC → L2/3I neuronal circuits and L2/3, L5, and L6 pyramidal neurons

Presynaptic interneurons	L2/3 pyramidal neurons (mV)	L5 pyramidal neurons (mV)	L6 pyramidal neurons (mV)
SBC→	0.043 ± 0.008 ($n = 3$)	0.030 ($n = 1$)	—
SBC→MaC→	0.424 ± 0.009 ($n = 23$)	0.238 ± 0.016 ($n = 8$)	—
SBC→NGC→	0.620 ± 0.004 ($n = 97$)	0.320 ± 0.003 ($n = 97$)	—
SBC→BTC→	0.437 ± 0.004 ($n = 119$)	0.289 ± 0.003 ($n = 93$)	—
SBC→BPC→	0.271 ± 0.018 ($n = 8$)	0.147 ± 0.014 ($n = 6$)	—
SBC→BaC→	0.633 ± 0.006 ($n = 75$)	0.414 ± 0.007 ($n = 52$)	—
SBC→DBC→	0.670 ± 0.013 ($n = 43$)	0.454 ± 0.005 ($n = 56$)	—
SBC→ChC→	0.586 ± 0.029 ($n = 11$)	0.287 ± 0.017 ($n = 7$)	—

section examination showed that the majority of light microscopically identified synaptic boutons were bona fide synapses (~80%; $n = 61$ of 77 boutons from 14 interneurons) with symmetric membrane profiles (Fig. 6*A–C* and Table 21). These results are consistent with the notion that light microscopically identified synaptic boutons are reliable indicators of synapses (Markram et al. 1997; Tamas et al. 2003; Jiang et al. 2013). Collectively, these results indicate that SBC → L2/3 interneuronal circuits control inhibition on both apical and oblique/basal dendritic domains of pyramidal neurons, whereas ENGC ↔ L2/3

Table 5
Synaptic connectivity between ENGC ↔ L2/3I neuronal circuits and L2/3, L5, and L6 pyramidal neurons

Presynaptic interneurons	L2/3 pyramidal neurons (connected/tested and %)		L5 pyramidal neurons (connected/tested and %)		L6 pyramidal neurons (connected/tested and %)	
ENGC→	153/243	63.0	28/138	20.3	0/65	0.0
$_{ENGC}$→MaC→	9/33	27.3	2/37	5.4	0/21	0.0
$_{ENGC}$→NGC→	83/175	47.4	52/206	25.2	0/72	0.0
$_{ENGC}$→BTC→	51/202	25.2	30/268	11.2	0/100	0.0

Table 6
Synaptic strength between ENGC ↔ L2/3I neuronal circuits and L2/3, L5, and L6 pyramidal neurons

Presynaptic interneurons	L2/3 pyramidal neurons (mV)	L5 pyramidal neurons (mV)	L6 pyramidal neurons (mV)
ENGC→	0.489 ± 0.003 (n = 109)	0.234 ± 0.005 (n = 22)	—
$_{ENGC}$→MaC→	0.448 ± 0.023 (n = 9)	0.150 (n = 2)	—
$_{ENGC}$→NGC→	0.558 ± 0.014 (n = 26)	0.218 ± 0.014 (n = 16)	—
$_{ENGC}$→BTC→	0.472 ± 0.014 (n = 19)	0.209 ± 0.020 (n = 10)	—

Table 7
Comparison of synaptic connectivity between SBC → L2/3I → L2P and →L3P neuronal circuits

Presynaptic interneurons	L2 pyramidal neurons (connected/tested and %)		L3 pyramidal neurons (connected/tested and %)		χ^2 and P value	
SBC→	2/206	0.9	1/357	0.3	1.176	0.278
$_{SBC}$→MaC→	14/39	35.9	10/49	20.4	2.627	0.105
$_{SBC}$→NGC→	68/105	64.8	107/149	71.8	1.429	0.232
$_{SBC}$→BTC→	76/218	34.9	106/294	36.1	0.078	0.781
$_{SBC}$→BPC→	4/39	10.3	4/63	6.3	0.509	0.476
$_{SBC}$→BaC→	52/146	35.6	53/176	30.1	1.100	0.294
$_{SBC}$→DBC→	27/63	42.9	26/83	31.3	2.060	0.151
$_{SBC}$→ChC→	8/29	27.6	5/44	11.4	3.143	0.076

Table 8
Comparison of synaptic connectivity between SBC → L2/3I → L5aP and →L5bP neuronal circuits

Presynaptic interneurons	L5a pyramidal neurons (connected/tested and %)		L5b pyramidal neurons (connected/tested and %)		χ^2 and P value	
SBC→	1/301	0.3	0/323	0.0	1.075	0.300
$_{SBC}$→MaC→	4/66	6.1	4/89	4.5	0.190	0.663
$_{SBC}$→NGC→	65/179	36.3	92/293	31.4	1.208	0.272
$_{SBC}$→BTC→	45/404	11.1	71/688	10.3	0.180	0.672
$_{SBC}$→BPC→	3/79	3.8	3/105	2.9	0.126	0.722
$_{SBC}$→BaC→	23/136	16.9	34/255	13.3	0.912	0.340
$_{SBC}$→DBC→	20/95	21.1	26/126	18.5	0.234	0.628
$_{SBC}$→ChC→	3/61	4.9	4/95	4.2	0.043	0.835

Table 9
Comparison of synaptic strength between SBC → L2/3I → L2P and →L3P neuronal circuits

Presynaptic interneurons	L2 pyramidal neurons (mV)	L3 pyramidal neurons (mV)	U and P value (M–W rank sum)	
SBC→	0.045 (n = 2)	0.040 (n = 1)	—	—
$_{SBC}$→MaC→	0.428 ± 0.014 (n = 14)	0.418 ± 0.025 (n = 9)	67.0	0.825
$_{SBC}$→NGC→	0.637 ± 0.011 (n = 46)	0.605 ± 0.007 (n = 51)	1262.0	0.523
$_{SBC}$→BTC→	0.414 ± 0.010 (n = 56)	0.457 ± 0.006 (n = 63)	2010.5	0.190
$_{SBC}$→BPC→	0.285 ± 0.043 (n = 4)	0.257 ± 0.035 (n = 4)	10.0	0.872
$_{SBC}$→BaC→	0.656 ± 0.010 (n = 36)	0.613 ± 0.013 (n = 39)	599.5	0.279
$_{SBC}$→DBC→	0.687 ± 0.029 (n = 24)	0.648 ± 0.021 (n = 19)	250.5	0.590
$_{SBC}$→ChC→	0.610 ± 0.025 (n = 7)	0.545 ± 0.069 (n = 4)	14.0	0.999

Table 10
Comparison of synaptic strength between SBC → L2/3I → L5aP and →L5bP neuronal circuits

Presynaptic interneurons	L5a pyramidal neurons (mV)	L5b pyramidal neurons (mV)	U and P value (M–W rank sum)	
SBC→	0.030 (n = 1)	—	—	—
$_{SBC}$→MaC→	0.228 ± 0.030 (n = 4)	0.248 ± 0.039 (n = 4)	7.0	0.886
$_{SBC}$→NGC→	0.298 ± 0.006 (n = 48)	0.334 ± 0.004 (n = 78)	1986.5	0.567
$_{SBC}$→BTC→	0.273 ± 0.006 (n = 39)	0.300 ± 0.004 (n = 54)	1158.5	0.413
$_{SBC}$→BPC→	0.168 ± 0.034 (n = 3)	0.127 ± 0.027 (n = 3)	7.0	0.400
$_{SBC}$→BaC→	0.429 ± 0.012 (n = 36)	0.378 ± 0.011 (n = 17)	265.5	0.446
$_{SBC}$→DBC→	0.462 ± 0.008 (n = 36)	0.438 ± 0.013 (n = 20)	370.5	0.376
$_{SBC}$→ChC→	0.283 ± 0.037 (n = 3)	0.290 ± 0.035 (n = 4)	6.0	0.999

Table 11
Comparison of synaptic connectivity between ENGC ↔ L2/3I → L2P and →L3P neuronal circuits

Presynaptic interneurons	L2 pyramidal neurons (connected/tested and %)		L3 pyramidal neurons (connected/tested and %)		χ^2 and P value	
ENGC→	67/112	59.8	86/131	65.6	0.879	0.348
$_{ENGC}$↔MaC→	4/12	33.3	5/21	23.8	0.349	0.555
$_{ENGC}$↔NGC→	45/83	54.2	38/92	41.3	2.918	0.088
$_{ENGC}$↔BTC→	24/106	28.1	27/96	22.6	0.803	0.370

Table 12
Comparison of synaptic connectivity between ENGC ↔ L2/3I → L5aP and →L5bP neuronal circuits

Presynaptic interneurons	L5a pyramidal neurons (connected/tested and %)		L5b pyramidal neurons (connected/tested and %)		χ^2 and P value	
ENGC→	11/59	18.6	17/79	21.5	0.173	0.678
$_{ENGC}$↔MaC→	1/23	4.3	1/14	7.1	0.133	0.715
$_{ENGC}$↔NGC→	32/108	29.6	20/98	20.4	2.315	0.128
$_{ENGC}$↔BTC→	16/123	13.0	14/145	9.7	0.753	0.386

Table 13
Comparison of synaptic strength between ENGC ↔ L2/3I → L2P and →L3P neuronal circuits

Presynaptic interneurons	L2 pyramidal neurons (mV)	L3 pyramidal neurons (mV)	U and P value (M–W rank sum)	
ENGC→	0.517 ± 0.005 (n = 58)	0.457 ± 0.006 (n = 51)	1696.0	0.188
$_{ENGC}$↔MaC→	0.418 ± 0.063 (n = 4)	0.472 ± 0.040 (n = 5)	11.0	0.905
$_{ENGC}$↔NGC→	0.585 ± 0.035 (n = 12)	0.535 ± 0.023 (n = 14)	82.5	0.959
$_{ENGC}$↔BTC→	0.462 ± 0.037 (n = 9)	0.281 ± 0.027 (n = 10)	48.5	0.806

Table 14
Comparison of synaptic strength between ENGC ↔ L2/3I → L5aP and →L5bP neuronal circuits

Presynaptic interneurons	L5a pyramidal neurons (mV)	L5b pyramidal neurons (mV)	U and P value (M–W rank sum)	
ENGC→	0.241 ± 0.009 (n = 14)	0.228 ± 0.010 (n = 12)	52.0	0.620
$_{ENGC}$↔MaC→	0.130 (n = 1)	0.170 (n = 1)	—	—
$_{ENGC}$↔NGC→	0.230 ± 0.010 (n = 8)	0.206 ± 0.009 (n = 8)	39.0	0.505
$_{ENGC}$↔BTC→	0.189 ± 0.022 (n = 6)	0.238 ± 0.073 (n = 4)	13.0	0.762

interneuronal circuits control inhibition of the apical dendritic domains of pyramidal neurons (Fig. 6*D*).

Discussion

In this study, we have established the connection patterns of cortical L1 neuron-led transsynaptic neuronal circuits that target different types of pyramidal neurons in supragranular

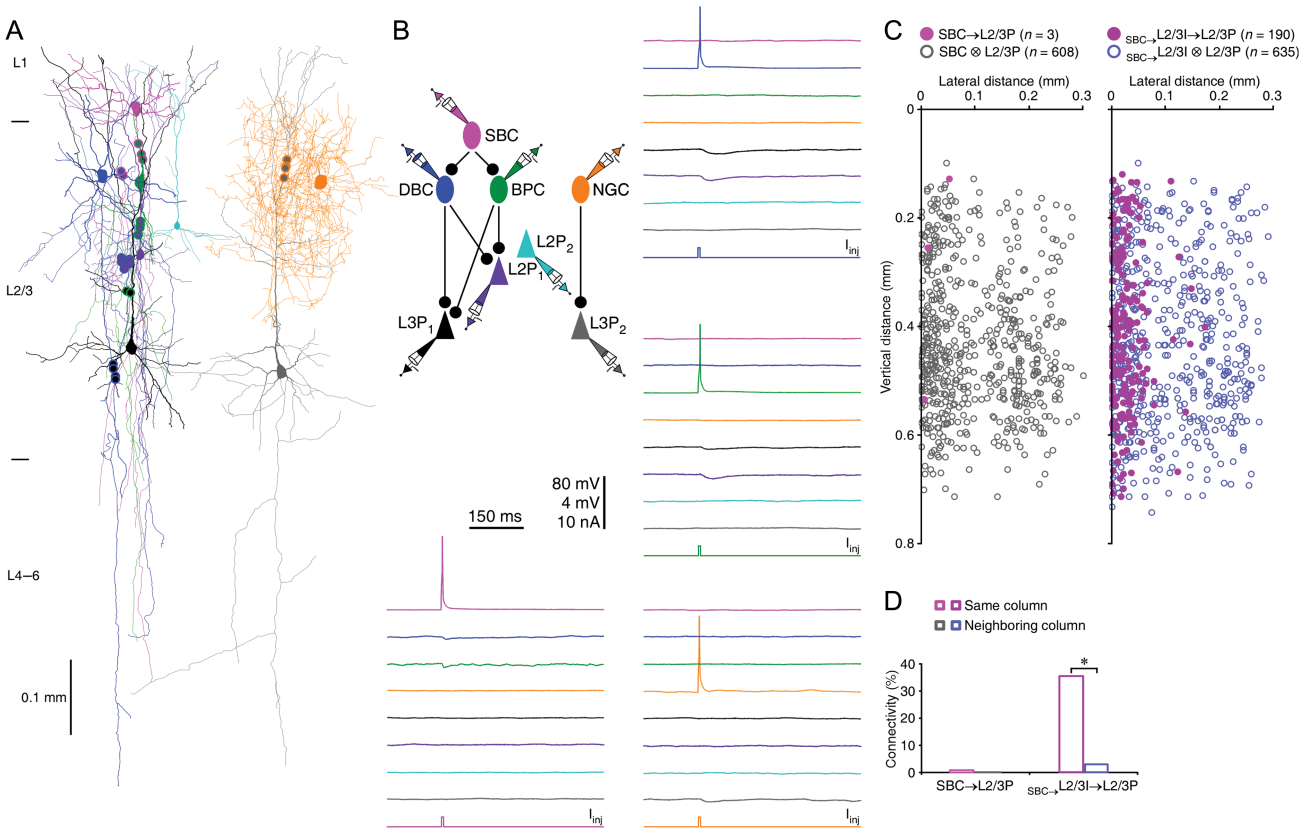

Figure 3. SBC → L2/3 interneuronal circuits inhibit L2/3 pyramidal neurons within single columns. (*A*) Reconstruction of L1 SBC (pink), L2 BPC (dark green), L2 DBC (blue), and multiple L2/3 pyramidal neurons (cyan, purple and black) in the same column, and L2 NGC (brown) and L3 pyramidal neuron (gray) in a neighboring column recorded simultaneously from an acute cortical slice. The double colored dots indicate the putative synaptic contacts based on anatomical reconstruction. (*B*) Single action potentials elicited in presynaptic SBC evoked uIPSPs in postsynaptic BPC and DBC, those in presynaptic BPC and DBC evoked uIPSPs in 2 postsynaptic L2/3 pyramidal neurons (purple and black), and those in presynaptic NGC evoked uIPSPs in postsynaptic L3 pyramidal neuron (gray). The schematic drawing shows symbolically the synaptic connections. Scale bars apply to all recording traces with 80 and 4 mV bars applied to traces with and without action potentials, respectively. (*C*) The plots show the relative position of L2/3 pyramidal neurons to SBCs and connectivity between SBCs or L2/3 interneurons innervated by SBCs and L2/3 pyramidal neurons. Note the origin of X and Y axes indicating the soma location of SBCs and the pia, filled and empty dots representing connected and unconnected neurons, respectively, and the region with reduced cell density correlating roughly with the border of columns. (*D*) Values for the connectivity of SBC → L2/3P (SBC → $L2/3P_{Same\ column}$: 0.9%, $n = 3$ of 353 tested connections; SBC → $L2/3P_{Neighboring\ column}$: 0.0%, $n = 0$ of 258 tested connections; $\chi^2 = 2.203$; $P = 0.14$) and $_{SBC\rightarrow}$L2/3I → L2/3P ($_{SBC\rightarrow}$L2/3I → $L2/3P_{Same\ column}$: 35.3%, $n = 190$ of 530 tested connections; $_{SBC\rightarrow}$L2/3I → $L2/3P_{Neighboring\ column}$: 2.7%, $n = 8$ of 294 tested connections; $\chi^2 = 111.095$; $P < 0.0005$). Asterisks indicate $P < 0.05$ (χ^2-tests).

and infragranular layers of the rat barrel cortex (Fig. 6*D*). Although these cortical interneuronal circuits exhibit a few cell type-specific variations in connectivity parameters, they generally display highly stereotypical connectivity, underscoring the canonical organization of cortical interneuronal circuits.

Canonical Organization of Cortical Interneuronal Circuits

SBCs and ENGCs, strategically located in cortical L1, are ideal for processing attentional and salient signals (Cauller et al. 1998; Gonchar and Burkhalter 2003; Petreanu et al. 2009; Rubio-Garrido et al. 2009; Letzkus et al. 2011; Jiang et al. 2013). This is because L1 receives inputs primarily from neurons in higher-order thalamic relays and higher-order cortical areas, and neurons in these areas preferentially increase their activity during attention-demanding processes (e.g., attentional, expectational, perceptual, and working memory tasks), and experimental manipulation of the activity of the neurons interferes with attentional tasks (Robinson and Petersen 1992; Tomita et al. 1999; Pascual-Leone and Walsh 2001; Gilbert and Sigman 2007; van Boxtel et al. 2010; Baluch and Itti 2011; Purushothaman et al. 2012; van Gaal and Lamme 2012; Larkum 2013). Consistent with this idea, in vivo recordings have shown that L1 inputs generate direct, rapid excitatory postsynaptic potentials in SBCs and ENGCs (Zhu and Zhu 2004; Jiang et al. 2013), and the excitation is selectively and dramatically enhanced during attentional tasks (Cauller and Kulics 1991; Kuhn et al. 2008; Letzkus et al. 2011). Moreover, L1 also receives dense innervations from neuromodulatory systems, and L1 interneurons respond robustly to various neuromodulators (Christophe et al. 2002; Yuen and Yan 2009; Letzkus et al. 2011). Finally, L1 SBCs and ENGCs seem able to effectively convert the attentional and salient signals via transsynaptic inhibitory and disinhibitory interneuronal circuits to govern salience selection in cortical output pyramidal neurons (Larkum et al. 1999; Larkum and Zhu 2002; Zhu and Zhu 2004; Jiang et al. 2013). We report here that cortical L1 neuron-led interneuronal circuits target pyramidal neurons in both supragranular and infragranular layers. These circuits exhibit a few cell type- and layer-dependent specificities. In general, the circuits form more and stronger inhibitory connections with supragranular L2 and L3 pyramidal neurons than infragranular L5a and L5b pyramidal neurons, and they do not form inhibitory connections with L6 pyramidal neurons. The density of

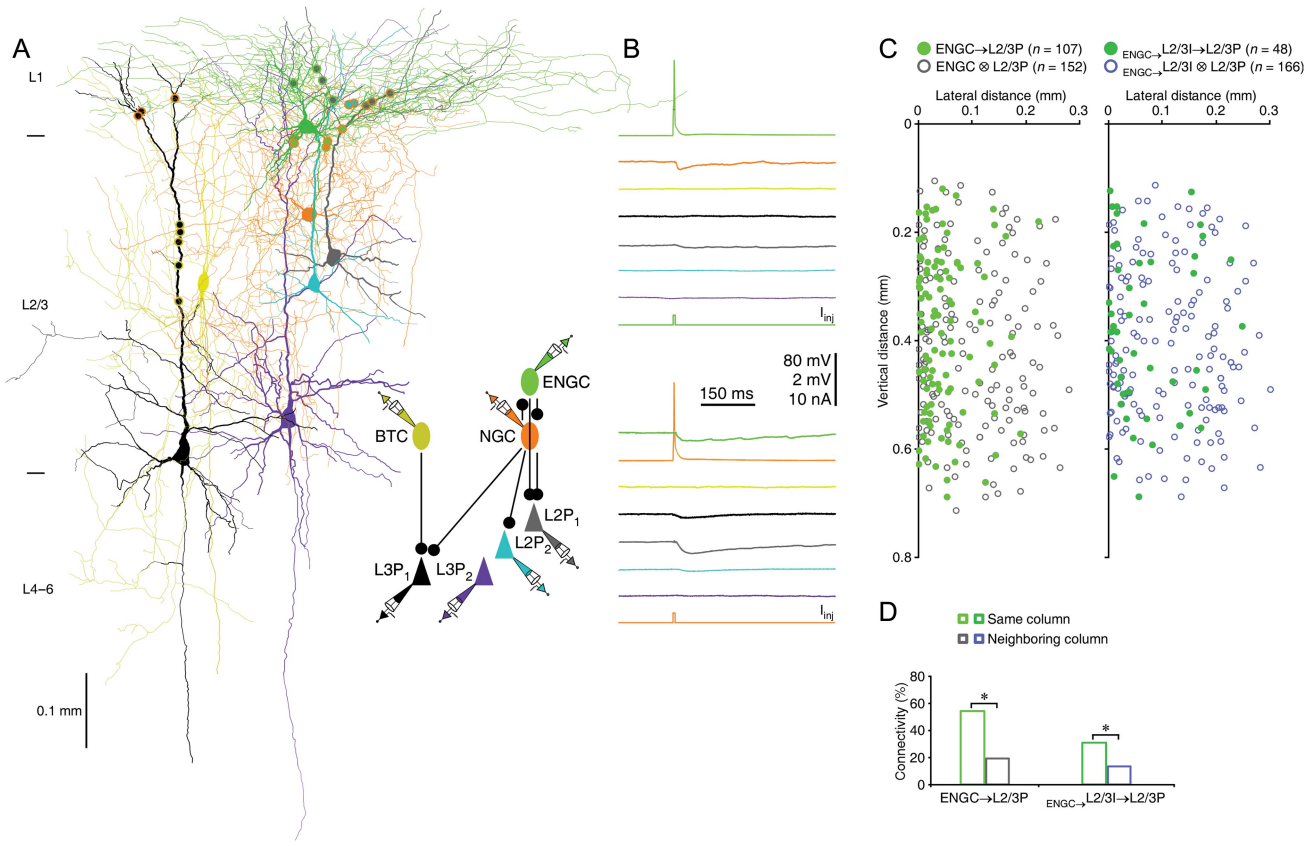

Figure 4. ENGCs ↔ L2/3 interneuronal circuits inhibit L2/3 pyramidal neurons across multiple columns. (*A*) Reconstruction of L1 ENGC (green), L2 NGC (brown), and multiple L2/3 pyramidal neurons (gray, cyan, and purple) in the same column, and L2/3 BTC (yellow) and L3 pyramidal neuron (black) in a neighboring column recorded simultaneously. The double colored dots indicate the putative synaptic contacts based on anatomical reconstruction. The schematic drawing shows symbolically the synaptic connections. (*B*) Single action potentials elicited in presynaptic ENGC and NGC evoked uIPSPs in postsynaptic NGC, ENGC, and 2 L2 pyramidal neurons (gray and cyan). Scale bars apply to all recording traces with 80 and 2 mV bars applied to traces with and without action potentials, respectively. (*C*) The plots show the relative position of L2/3 pyramidal neurons to ENGCs and connectivity between ENGCs or L2/3 interneurons innervated by ENGCs and L2/3 pyramidal neurons. Note the origin of *X* and *Y* axes indicating the soma location of ENGCs and the pia, filled and empty dots representing connected and unconnected neurons, respectively, and the region with reduced cell density correlating roughly with the border of columns. (*D*) Values for the connectivity of ENGC → L2/3P (ENGC → $L2/3P_{Same\ column}$: 54.3%, $n = 89$ of 164 tested connections; ENGC → $L2/3P_{Neighboring\ column}$: 18.9%, $n = 18$ of 95 tested connections; $\chi^2 = 30.953$; $P < 0.0005$) and $_{ENGC}$↔L2/3I → L2/3P ($_{ENGC}$↔L2/3I → $L2/3P_{Same\ column}$: 30.7%, $n = 35$ of 114 tested connections; $_{ENGC}$↔L2/3I → $L2/3P_{Neighboring\ column}$: 13.0%, $n = 13$ of 100 tested connections; $\chi^2 = 9.594$; $P < 0.005$). Asterisks indicate $P < 0.05$ (χ^2-tests).

Table 15
Comparison of synaptic connectivity of SBC → L2/3I → L2/3P neuronal circuits between columns

Cell connection pattern	L2/3P in same columns (connected/tested and %)		L2/3P in neighboring columns (connected/tested and %)		χ^2 and *P* value	
SBC → L2P	2/137	1.5	0/93	0.0	1.370	0.242
$_{SBC}$→L2/3I → L2P	93/245	38.0	4/115	3.5	47.271	<0.0005
SBC → L3P	1/216	0.5	0/165	0.0	0.766	0.381
$_{SBC}$→L2/3I → L3P	97/294	33.0	4/179	2.2	62.680	<0.0005

Table 16
Comparison of synaptic connectivity of SBC → L2/3I → L5P neuronal circuits between columns

Cell connection pattern	L5P in same columns (connected/tested and %)		L5P in neighboring columns (connected/tested and %)		χ^2 and *P* value	
SBC → L5aP	1/114	0.9	0/63	0.0	0.571	0.450
$_{SBC}$→L2/3I → L5aP	30/209	14.4	0/102	0.0	16.204	<0.0005
SBC → L5bP	0/118	0.0	0/69	0.0	2.289	—
$_{SBC}$→L2/3I → L5bP	24/250	9.6	0/133	0.0	13.622	<0.0005

Table 17
Comparison of synaptic connectivity of ENGC ↔ L2/3I → L2/3P neuronal circuits between columns

Cell connection pattern	L2/3P in same columns (connected/tested and %)		L2/3P in neighboring columns (connected/tested and %)		χ^2 and *P* value	
ENGC → L2P	49/85	57.6	10/40	25.0	11.633	<0.005
$_{ENGC}$→L2/3I → L2P	21/59	35.6	7/46	15.2	5.488	<0.05
ENGC → L3P	40/79	50.6	8/55	14.5	18.368	<0.0005
$_{ENGC}$→L2/3I → L3P	14/55	25.5	6/54	11.1	3.742	0.053

Table 18
Comparison of synaptic connectivity of ENGC ↔ L2/3I → L5P neuronal circuits between columns

Cell connection pattern	L5P in same columns (connected/tested and %)		L5P in neighboring columns (connected/tested and %)		χ^2 and *P* value	
ENGC → L5aP	13/76	17.1	2/22	9.1	0.845	0.358
$_{ENGC}$→L2/3I → L5aP	8/77	10.4	0/30	0.0	3.369	0.066
ENGC → L5bP	22/96	22.9	3/25	12.0	1.442	0.230
$_{ENGC}$→L2/3I → L5bP	7/86	8.1	0/34	0.0	2.939	0.086

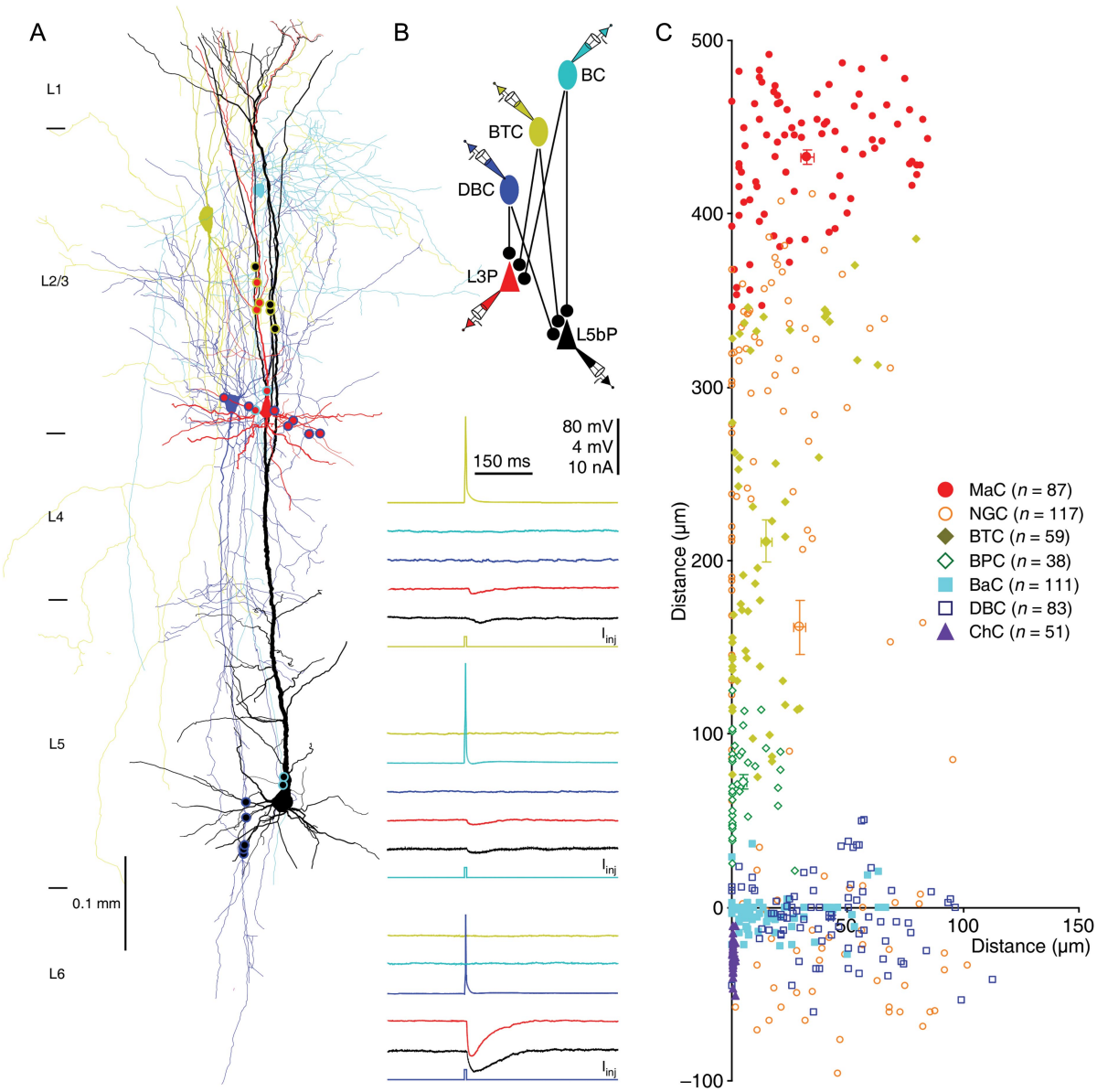

Figure 5. L2/3 interneurons target different compartments of L2/3 pyramidal neurons. (*A*) Reconstruction of L2 BTC (yellow), L2 BaC (cyan), L3 DBC (blue), and L3 and L5 pyramidal neurons (red and black) recorded simultaneously from an acute cortical slice. The double colored dots indicate the putative synaptic contacts based on anatomical reconstruction. (*B*) Single action potentials elicited in presynaptic BTC, BaC and DBC evoked uIPSPs in postsynaptic L3 and L5 pyramidal neurons, respectively. The above schematic drawing shows symbolically the synaptic connections. Scale bars apply to all recording traces with 80 and 4 mV bars applied to traces with and without action potentials, respectively. (*C*) The coordinates, or the horizontal and vertical distance of the synapses made by seven groups of L2/3 interneurons from the soma of L2/3 pyramidal neurons (see Table 19 for values).

axonal arborization of L2/3 interneurons, which appears to correlate with the connectivity of these interneurons to L2/3, L5 and L6 pyramidal neurons, seems to be the primary determinant of this connectivity pattern. Truncation of axons of interneurons and apical dendrites of L5–6 pyramidal neurons, for example, induced by slicing procedure, could exaggerate the laminar-dependent differences in connectivity. However, this contribution is likely to be limited because the cortical slices used in this study are parallel or near parallel to (<~4°) apical dendrites of L5–6 pyramidal neurons and the axonal arborization of the majority of L2/3 interneurons remains largely intact in L5 and L6 (Figs 1–5; see also Jiang et al. 2013). This is supported by the results that there is no significant difference in connectivity between L2 and L3 pyramidal neurons or between L5a and L5b pyramidal neurons (Tables 7 and 8 and 11 and 12). Interestingly, NGCs innervated by SBCs, but not by ENGCs, form synapses on both apical and basal dendrites of L2/3 pyramidal neurons, whereas all NGCs, innervated by either SBCs or ENGCs, form synapses on apical dendrites of L5 pyramidal neurons. Furthermore, while SBC → L2/3 interneuronal circuits typically control inhibition of pyramidal neurons only in the same columns, they occasionally innervate L2/3 pyramidal neurons in neighboring columns. The functional significance of such connectivity variations is unclear, but the specificities likely reflect the functional specialization of L2, L3, L5a and L5b pyramidal neurons, which are differentially involved in cortical information processing (Zhu and Connors 1999; Brecht et al. 2003; Manns et al. 2004; Shepherd and Svoboda 2005).

We show here that cortical L1 neuron-led interneuronal circuits share many similarities in their connection diagrams

Table 19

Coordinates of synapses formed by SBC→ and ENGC ↔ L2/3I neuronal circuits on L2/3 pyramidal neurons

Presynaptic	L2 pyramidal neurons			L3 pyramidal neurons		
interneurons	$Coordinate_{lateral\ and\ vertical}$ (μm) and $N_{synapses\ and\ cells}$			$Coordinate_{lateral\ and\ vertical}$ (μm) and $N_{synapses\ and\ cells}$		
$_{SBC}$→MaC→	34.6 ± 6.4 (±61.6)	251.9 ± 5.3 (±85.3)	n = 23 (5 MaCs)	31.7 ± 3.0 (±47.3)	437.7 ± 4.2 (±66.6)	n = 64 (11 MaCs)
$_{SBC}$→NGC→	27.7 ± 2.3 (±46.0)	117.6 ± 14.2 (±139.1)	n = 45 (11 NGCs)	30.2 ± 3.6 (±61.4)	140.2 ± 20.6 (±332.3)	n = 72 (14 NGCs)
$_{SBC}$→BTC→	11.9 ± 2.2 (±27.9)	130.1 ± 9.6 (±162.5)	n = 26 (5 BTCs)	17.1 ± 3.5 (±40.6)	206.8 ± 17.8(±204.3)	n = 33 (10 BTCs)
$_{SBC}$→BPC→	4.6 ± 1.7 (±15.3)	45.0 ± 3.4 (±49.1)	n = 19 (4 BPCs)	5.2 ± 1.8 (±15.5)	70.7 ± 5.8 (±50.5)	n = 19 (4 BPCs)
$_{SBC}$→BaC→	14.9 ± 2.2 (±28.2)	−2.3 ± 1.0 (±21.7)	n = 41 (7 BaCs)	16.5 ± 2.4 (±39.4)	−3.5 ± 1.1 (±18.8)	n = 70 (17 BaCs)
$_{SBC}$→DBC→	44.5 ± 4.3 (±46.8)	−3.2 ± 1.8 (±32.8)	n = 30 (6 DBCs)	41.6 ± 3.7 (±53.8)	−4.4 ± 3.5 (±50.9)	n = 53 (12 DBCs)
$_{SBC}$→ChC→	0.2 ± 0.1 (±0.8)	−16.0 ± 1.0 (±17.9)	n = 29 (5 ChCs)	0.1 ± 0.1 (±0.6)	−25.8 ± 1.5 (±14.3)	n = 22 (4 ChCs)
ENGC→	31.7 ± 6.6 (±52.9)	209.8 ± 9.1 (±121.7)	n = 16 (4 ENGCs)	37.9 ± 5.3 (±51.9)	397.9 ± 8.6 (±88.7)	n = 24 (5 ENGCs)
$_{ENGC}$→MaC→	34.7 ± 6.5 (±57.1)	258.3 ± 4.7 (±68.9)	n = 19 (4 MaCs)	31.9 ± 4.6 (±49.1)	439.8 ± 5.9 (±63.6)	n = 29 (6 MaCs)
$_{ENGC}$→NGC→	24.3 ± 6.5 (±45.0)	187.9 ± 7.9 (±91.4)	n = 12 (3 NGCs)	24.8 ± 4.4 (±34.0)	313.1 ± 13.2 (±124.2)	n = 15 (4 NGCs)
$_{ENGC}$→ChC→	13.7 ± 4.6 (±32.0)	136.7 ± 10.7(±123.3)	n = 12 (3 BTCs)	17.1 ± 5.2 (±42.5)	246.3 ± 19.1 (±127.6)	n = 23 (5 BTCs)

Note: No significant difference in the relative coordinates of the synapses form by each L1–3 interneuron group on L2 and L3 pyramidal neurons ($P > 0.05$; Mann–Whitney rank-sum tests). The coordinates are present as mean ± SEM (±2SD that represents of the distribution range of 72.8% of data points).

Table 20

Coordinates of synapses formed by SBC→ and ENGC ↔ L2/3I neuronal circuits on L5 pyramidal neurons

Presynaptic interneurons	L5a pyramidal neurons			L5b pyramidal neurons		
	$Coordinate_{lateral\ and\ vertical}$ (μm) and $N_{synapses\ and\ cells}$			$Coordinate_{lateral\ and\ vertical}$ (μm) and $N_{synapses\ and\ cells}$		
$_{SBC}$→MaC→	34.3 ± 4.6 (±41.5)	794.3 ± 9.5 (±94.2)	n = 20 (4 MaCs)	34.6 ± 4.6 (±48.7)	971.3 ± 11.8 (±113.3)	n = 28 (5 MaCs)
$_{SBC}$→NGC→	27.3 ± 4.3 (±43.9)	697.9 ± 11.6 (±133.4)	n = 27 (7 NGCs)	27.9 ± 4.6 (±52.7)	851.2 ± 13.4 (±139.8)	n = 33 (5 NGCs)
$_{SBC}$→BTC→	5.4 ± 2.3 (±32.5)	597.6 ± 15.9 (±218.9)	n = 48 (9 BTCs)	7.3 ± 1.2 (±23.4)	661.0 ± 14.0 (±253.2)	n = 99 (12 BTCs)
$_{SBC}$→BPC→	14.3 ± 4.3 (±37.3)	268.3 ± 18.9 (±183.1)	n = 19 (4 BPCs)	15.8 ± 4.4 (±36.8)	330.2 ± 21.2 (±168.4)	n = 16 (4 BPCs)
$_{SBC}$→BaC→	11.9 ± 2.2 (±27.7)	−0.8 ± 1.8 (±26.0)	n = 41 (7 BaCs)	12.4 ± 1.6 (±22.7)	−0.7 ± 2.3 (±30.4)	n = 52 (12 BaCs)
$_{SBC}$→DBC→	52.5 ± 4.4 (±53.6)	−15.7 ± 7.9 (±106.3)	n = 37 (9 DBCs)	50.7 ± 3.0 (±42.7)	−17.8 ± 7.9 (±103.6)	n = 52 (10 DBCs)
$_{SBC}$→ChC→	0.0 ± 0.0 (±0.0)	−29.2 ± 1.6 (±12.0)	n = 11 (3 ChCs)	0.1 ± 0.1 (±0.6)	−32.9 ± 1.7 (±10.8)	n = 12 (3 ChCs)
ENGC→	42.7 ± 7.7 (±69.3)	780.0 ± 15.7 (±156.0)	n = 20 (4 ENGCs)	41.8 ± 5.2 (±50.1)	873.6 ± 15.6 (±149.4)	n = 23 (5 ENGCs)
$_{ENGC}$→MaC→	40.3 ± 7.7 (±57.4)	759.5 ± 12.2 (±101.7)	n = 14 (3 MaCs)	34.5 ± 7.2 (±51.8)	886.2 ± 14.5 (±104.3)	n = 13 (3 MaCs)
$_{ENGC}$→NGC→	28.7 ± 4.8 (±34.5)	704.7 ± 17.0 (±136.4)	n = 13 (3 NGCs)	31.9 ± 8.1 (±64.6)	784.9 ± 20.5 (±164.2)	n = 16 (5 NGCs)
$_{ENGC}$→ChC→	8.1 ± 3.7 (±31.9)	561.1 ± 31.6 (±306.4)	n = 19 (4 BTCs)	7.2 ± 2.2 (±18.3)	596.0 ± 37.6 (±310.3)	n = 17 (4 BTCs)

Note: No significant difference in the relative coordinates of the synapses form by each L1–3 interneuron group on L5a and L5b pyramidal neurons ($P > 0.05$; Mann–Whitney rank-sum tests). The coordinates are present as mean ± SEM (±2SD, which represents of the distribution range of 72.8% of data points).

(Fig. 6*D*). For example, both SBC- and ENGC-led interneuronal circuits selectively control inhibition of pyramidal neurons in L2/3 and L5, but not L6. Moreover, SBC → L2/3 interneuron → L2, →L3, →L5a, and →L5b pyramidal neuronal circuits are structured to inhibit both the apical and oblique/basal dendritic domains of a small number of pyramidal neurons, and they preferentially inhibit pyramidal neurons located within the same columns. Similarly, ENGC ↔ L2/3 interneuron → L2, →L3, →L5a, and →L5b pyramidal neuronal circuits are all constructed to inhibit only the apical dendritic domains of a large number of L2, L3, L5a, and L5b pyramidal neurons, and they commonly inhibit these pyramidal neurons across multiple columns. Finally, all L1 interneuron-led circuits target their synapses on specific subcellular compartments of pyramidal neurons in a L2/3 interneuron cell type-dependent manner, and together they cover all functional dendritic–somato–axonal compartments of pyramidal neurons (Reyes 2001; Sjostrom et al. 2008; Larkum 2013). The results suggest that axonal arborization patterns not only allow unambiguous classification of L2/3 interneurons but also reliably predict the specific circuit connections in which these L2/3 interneurons participate. The findings support the hypothesis that the axonal arborization-based interneuronal classification may represent a functional classification scheme (Markram et al. 2004). Collectively, our data, which demonstrate transsynaptic interneuronal circuit control of different pyramidal neurons in both cortical supragranular and infragranular layers, to our knowledge, provide the first evidence at the circuit level supporting the canonical organization of cortical interneuronal circuits.

Functional Implications of Canonical Cortical Interneuronal Circuits

The cortical L1 consists of sparsely distributed GABAergic interneurons that have somewhat overlapping electrophysiological properties (Chu et al. 2003; Zhu and Zhu 2004; Kubota et al. 2011; Wozny and Williams 2011; Cruikshank et al. 2012; Jiang et al. 2013; Ma et al. 2013). In addition, the molecular properties of L1 neurons remain poorly characterized and to some extent controversial (Kubota et al. 2011; Ma et al. 2013; Craig and McBain 2014). On the other hand, L1 interneurons exhibit 2 distinct axonal arborization patterns, that is, vertically descending horsetail-like axonal bundles versus horizontally elongated dense axonal arborizations, which can allow them to be unequivocally classified into 2 general groups, SBCs and ENGCs (Zhu and Zhu 2004; Jiang et al. 2013). These characteristic axonal arborization patterns seem ideally constructed to connect L1 interneurons into 2 largely independent interneuronal circuits (Jiang et al. 2013). Specifically, SBCs predominantly innervate interneurons vertically down in the deeper layers to head disinhibitory circuits, whereas ENGCs preferentially form mutual inhibitory and electric synapses with

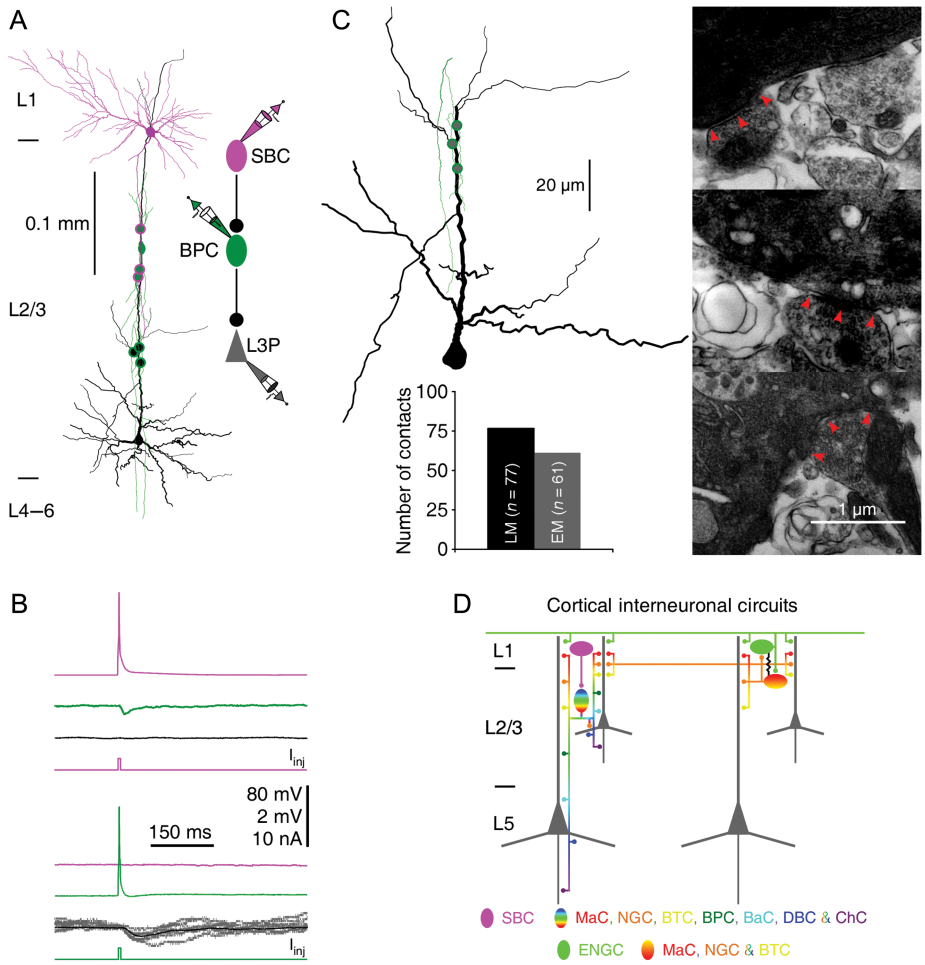

Figure 6. Electron microscopy confirms light microscopy-identified synaptic boutons. (*A*) Reconstruction of L1 SBC, L2/3 BPC (dark green), and L3 pyramidal neuron (black) recorded simultaneously from an acute cortical slice. The double colored dots indicate the putative synaptic contacts identified by LM. The schematic drawing shows symbolically the synaptic connections. (*B*) Single action potentials elicited in presynaptic SBC and BPC evoked uIPSPs in postsynaptic BPC and L3 pyramidal neuron, respectively. 80 and 2 mV bars apply to traces with and without action potentials, respectively. Note the average uIPSP trace (black), as well as superimposed individual uIPSP traces (gray). (*C*) Three light microscopy-identified synaptic boutons (left Neurolucida drawing) were confirmed with electron microscopy (right ultrastructure images). Arrow heads in EM images indicate synaptic junctions established by the axon of BPC. Inserted histograms summarize the numbers of light microscopy- and electron microscopy-identified synapses on L2/3 pyramidal neurons. (*D*) Schematic drawing shows key features of SBC→ and ENGC ↔ L2/3I → L2–5 pyramidal neuronal circuits. See the main text for the detailed architecture of the cortical interneuronal circuits.

Table 21
Correlation of LM- and EM-identified inhibitory synapses on L2/3 pyramidal neurons

Cell pair	No. of cell pairs	No. of LM-identified synapses	No. of EM-identified synapses	Confirmation rate (%)
MaC → L2/3P	2	13	11	84.6
NGC → L2/3P	2	10	7	70.0
BTC → L2/3P	3	16	12	75.0
BPC → L2/3P	1	3	3	100.0
BaC → L2/3P	3	19	14	73.7
DBC → L2/3P	2	11	10	90.9
ChC → L2/3P	1	6	4	80.0
Total	14	77	61	79.2

interneurons in L1 and superficial L2/3 across multiple columns to lead powerful inhibitory circuits (Letzkus et al. 2011; Palmer et al. 2012; Jiang et al. 2013; Pi et al. 2013). The correlation between the axonal arborization patterns of L1 interneurons and L1 interneuron-led neuronal circuits further supports the notion that the axonal arborization-based interneuronal classification may be used as an effective classification scheme (Markram et al. 2004). We show here that both SBC → L2/3 and ENGC ↔ L2/3 interneuronal circuits regulate inhibition of pyramidal neurons in L2/3 and L5, but not L6. Previous studies have shown that cortical L2, L3, L5a, and L5b pyramidal neurons process sensory information differently (Zhu and Connors 1999; Brecht et al. 2003; Manns et al. 2004; Shepherd and Svoboda 2005). For example, L2 pyramidal neurons respond to sensory inputs with a longer latency and a longer integration time than L3 pyramidal neurons, suggesting involvement of different degrees of local circuit integration (Feldmeyer et al. 2002; Brecht et al. 2003). On the other hand, L5a pyramidal neurons have more confined sub- and suprathreshold receptive fields than L5b pyramidal neurons, resulting from different combinations of sensory inputs from lemniscal and paralemniscal pathways (Manns et al. 2004; de Kock and Sakmann 2009). Interestingly, all such pyramidal neurons have 2 general input-receiving domains, an apical dendritic domain and an oblique/basal dendritic–somato–axonal domain, which primarily receive modulatory and sensory inputs, respectively (Zhu 2000, 2009; Larkum and Zhu

2002; Antic 2003; Petreanu et al. 2009). Moreover, these neurons can use a coincidence detection mechanism to selectively and non-linearly amplify near-synchronous inputs arriving at their apical and oblique/basal dendrites (Larkum et al. 1999, 2009; Larkum and Zhu 2002; Waters et al. 2003; Xu et al. 2012). Cortical interneuronal circuits play a dominant role in controlling the coincidence detection mechanism (Larkum et al. 1999; Jiang et al. 2013). The canonical SBC→ and ENGC ↔ L2/3 interneuron → L2–5 pyramidal neuronal circuits suggest that these interneuronal circuits use the same strategy to select salient information in L2, L3, L5a, and L5b pyramidal neurons. In particular, SBC → L2/3 interneuronal circuits enhance supralinear amplification of coincident inputs in a small population of spatially and temporally restricted L2/3 and L5 pyramidal neurons (Jiang et al. 2013). Moreover, ENGC ↔ L2/3 interneuronal circuits suppress amplification of coincident inputs in the majority of L2/3 and L5 pyramidal neurons over a large area, effectively augmenting the signal-to-noise ratio and sharpening the receptive field (Jiang et al. 2013). Furthermore, SBCs have a smaller receptive field with higher acuity than ENGCs (Zhu and Zhu 2004), which may produce a much smaller suprathreshold field (Anderson et al. 2000; Petersen et al. 2003; Zhu et al. 2004; Sun et al. 2010). Finally, during sensory processing, SBCs receive the earliest L1 inputs, respond rapidly, and can then quickly inactivate (Zhu and Zhu 2004), due presumably to the inhibition from interneurons in ENGC ↔ L2/3 interneuronal circuits (Chu et al. 2003; Wozny and Williams 2011; Jiang et al. 2013). Together, these results suggest that SBCs and ENGCs form stereotypical transsynaptic inhibitory circuits to control inhibitions of pyramidal neurons throughout L2–5 and that these canonical circuits seem designed to effectively amplify highly defined spatial and temporal signals in both supragranular and infragranular layers.

Supplementary Material

Supplementary material can be found at: http://www.cercor.oxfordjournals.org/.

Funding

This study was supported in part by a undergraduate research award from the Center for Undergraduate Excellence of the University of Virginia (A.J.L.), postdoctoral fellowships from the Epilepsy Foundation (G.W. and X.J.), SAFEA Cultural and Educational Expert Award (Y.S. and J.J.Z.), Chinese Ministry of Education Project 111 Program B13026 (M.P.B., Y.S., and J.J.Z.), and the US National Institutes of Health. This paper is the part of a dissertation in partial fulfillment of the requirements of the BS degree (A.J.L.) at the University of Virginia.

Notes

We thank Drs Ed Callaway, Alev Erisir, Karel Svoboda and Gabor Tamas for technical advice and invaluable discussions, and members of the Zhu laboratory for comments and technical assistance. *Conflict of Interest*: None declared.

References

Agmon A, Connors BW. 1991. Thalamocortical responses of mouse somatosensory (barrel) cortex in vitro. Neuroscience. 41:365–379.

Anderson JS, Lampl I, Gillespie DC, Ferster D. 2000. The contribution of noise to contrast invariance of orientation tuning in cat visual cortex. Science. 290:1968–1972.

Antic SD. 2003. Action potentials in basal and oblique dendrites of rat neocortical pyramidal neurons. J Physiol. 550:35–50.

Ascoli GA, Alonso-Nanclares L, Anderson SA, Barrionuevo G, Benavides-Piccione R, Burkhalter A, Buzsaki G, Cauli B, Defelipe J, Fairen A et al. 2008. Petilla terminology: nomenclature of features of GABAergic interneurons of the cerebral cortex. Nat Rev Neurosci. 9:557–568.

Baluch F, Itti L. 2011. Mechanisms of top-down attention. Trends Neurosci. 34:210–224.

Batista-Brito R, Fishell G. 2009. The developmental integration of cortical interneurons into a functional network. Curr Top Dev Biol. 87:81–118.

Brecht M, Roth A, Sakmann B. 2003. Dynamic receptive fields of reconstructed pyramidal cells in layers 3 and 2 of rat somatosensory barrel cortex. J Physiol. 553:243–265.

Cauller LJ, Clancy B, Connors BW. 1998. Backward cortical projections to primary somatosensory cortex in rats extend long horizontal axons in layer I. J Comp Neurol. 390:297–310.

Cauller LJ, Kulics AT. 1991. The neural basis of the behaviorally relevant N1 component of the somatosensory-evoked potential in SI cortex of awake monkeys: evidence that backward cortical projections signal conscious touch sensation. Experimental Brain Research Experimentelle Hirnforschung Experimentation Cerebrale. 84:607–619.

Christophe E, Roebuck A, Staiger JF, Lavery DJ, Charpak S, Audinat E. 2002. Two types of nicotinic receptors mediate an excitation of neocortical layer I interneurons. J Neurophysiol. 88:1318–1327.

Chu Z, Galarreta M, Hestrin S. 2003. Synaptic interactions of late-spiking neocortical neurons in layer 1. J Neurosci. 23:96–102.

Craig MT, McBain CJ. 2014. The emerging role of GABAB receptors as regulators of network dynamics: fast actions from a 'slow' receptor? Curr Opin Neurobiol. 26:15–21.

Cruikshank SJ, Ahmed OJ, Stevens TR, Patrick SL, Gonzalez AN, Elmaleh M, Connors BW. 2012. Thalamic control of layer 1 circuits in prefrontal cortex. J Neurosci. 32:17813–17823.

de Kock CP, Sakmann B. 2009. Spiking in primary somatosensory cortex during natural whisking in awake head-restrained rats is cell-type specific. Proc Natl Acad Sci USA. 106:16446–16450.

Douglas RJ, Martin KA. 2007. Mapping the matrix: the ways of neocortex. Neuron. 56:226–238.

Feldmeyer D, Lubke J, Silver RA, Sakmann B. 2002. Synaptic connections between layer 4 spiny neurone-layer 2/3 pyramidal cell pairs in juvenile rat barrel cortex: physiology and anatomy of interlaminar signalling within a cortical column. J Physiol. 538:803–822.

Gilbert CD, Sigman M. 2007. Brain states: top-down influences in sensory processing. Neuron. 54:677–696.

Gilbert CD, Wiesel TN. 1983. Functional organization of the visual cortex. Prog Brain Res. 58:209–218.

Gonchar Y, Burkhalter A. 2003. Distinct GABAergic targets of feedforward and feedback connections between lower and higher areas of rat visual cortex. J Neurosci. 23:10904–10912.

Huang ZJ, Di Cristo G, Ango F. 2007. Development of GABA innervation in the cerebral and cerebellar cortices. Nat Rev Neurosci. 8:673–686.

Ito M. 1992. Simultaneous visualization of cortical barrels and horseradish peroxidase-injected layer 5b vibrissa neurones in the rat. J Physiol. 454:247–265.

Jiang X, Wang G, Lee AJ, Stornetta RL, Zhu JJ. 2013. The organization of two new cortical interneuronal circuits. Nat Neurosci. 16:210–218.

Katzel D, Zemelman BV, Buetfering C, Wolfel M, Miesenbock G. 2011. The columnar and laminar organization of inhibitory connections to neocortical excitatory cells. Nat Neurosci. 14:100–107.

Kielland A, Bochorishvili G, Corson J, Zhang L, Rosin DL, Heggelund P, Zhu JJ. 2009. Activity patterns govern synapse-specific AMPA-R trafficking between deliverable and synaptic pools. Neuron. 62:84–101.

Kubota Y. 2014. Untangling GABAergic wiring in the cortical microcircuit. Curr Opin Neurobiol. 26:7–14.

Kubota Y, Shigematsu N, Karube F, Sekigawa A, Kato S, Yamaguchi N, Hirai Y, Morishima M, Kawaguchi Y. 2011. Selective coexpression of multiple chemical markers defines discrete populations of neocortical GABAergic neurons. Cereb Cortex. 21:1803–1817.

Kuhn B, Denk W, Bruno RM. 2008. In vivo two-photon voltage-sensitive dye imaging reveals top-down control of cortical layers 1 and 2 during wakefulness. Proc Natl Acad Sci USA. 105:7588–7593.

Larkum M. 2013. A cellular mechanism for cortical associations: an organizing principle for the cerebral cortex. Trends Neurosci. 36:141–151.

Larkum ME, Nevian T, Sandler M, Polsky A, Schiller J. 2009. Synaptic integration in tuft dendrites of layer 5 pyramidal neurons: a new unifying principle. Science. 325:756–760.

Larkum ME, Zhu JJ. 2002. Signaling of layer 1 and whisker-evoked Ca^{2+} and Na^{+} action potentials in distal and terminal dendrites of rat neocortical pyramidal neurons in vitro and in vivo. J Neurosci. 22:6991–7005.

Larkum ME, Zhu JJ, Sakmann B. 1999. A new cellular mechanism for coupling inputs arriving at different cortical layers. Nature. 398:338–341.

Letzkus JJ, Wolff SB, Meyer EM, Tovote P, Courtin J, Herry C, Luthi A. 2011. A disinhibitory microcircuit for associative fear learning in the auditory cortex. Nature. 480:331–335.

Ma J, Yao XH, Fu Y, Yu YC. 2013. Development of layer 1 neurons in the mouse neocortex. Cereb Cortex. [Epub ahead of print].

Manns ID, Sakmann B, Brecht M. 2004. Sub- and suprathreshold receptive field properties of pyramidal neurones in layers 5A and 5B of rat somatosensory barrel cortex. J Physiol. 556:601–622.

Markram H, Lubke J, Frotscher M, Roth A, Sakmann B. 1997. Physiology and anatomy of synaptic connections between thick tufted pyramidal neurones in the developing rat neocortex. J Physiol (Lond). 500:409–440.

Markram H, Toledo-Rodriguez M, Wang Y, Gupta A, Silberberg G, Wu C. 2004. Interneurons of the neocortical inhibitory system. Nat Rev Neurosci. 5:793–807.

Meyer HS, Wimmer VC, Oberlaender M, de Kock CP, Sakmann B, Helmstaedter M. 2010. Number and laminar distribution of neurons in a thalamocortical projection column of rat vibrissal cortex. Cereb Cortex. 20:2277–2286.

Mountcastle VB. 1997. The columnar organization of the neocortex. Brain. 120:701–722.

Nassi JJ, Callaway EM. 2009. Parallel processing strategies of the primate visual system. Nat Rev Neurosci. 10:360–372.

Palmer LM, Schulz JM, Murphy SC, Ledergerber D, Murayama M, Larkum ME. 2012. The cellular basis of $GABA_B$-mediated interhemispheric inhibition. Science. 335:989–993.

Pascual-Leone A, Walsh V. 2001. Fast backprojections from the motion to the primary visual area necessary for visual awareness. Science. 292:510–512.

Petersen CC. 2007. The functional organization of the barrel cortex. Neuron. 56:339–355.

Petersen CC, Hahn TT, Mehta M, Grinvald A, Sakmann B. 2003. Interaction of sensory responses with spontaneous depolarization in layer 2/3 barrel cortex. Proc Natl Acad Sci USA. 100:13638–13643.

Petreanu L, Mao T, Sternson SM, Svoboda K. 2009. The subcellular organization of neocortical excitatory connections. Nature. 457:1142–1145.

Pfeffer CK, Xue M, He M, Huang ZJ, Scanziani M. 2013. Inhibition of inhibition in visual cortex: the logic of connections between molecularly distinct interneurons. Nat Neurosci. 16:1068–1076.

Pi HJ, Hangya B, Kvitsiani D, Sanders JI, Huang ZJ, Kepecs A. 2013. Cortical interneurons that specialize in disinhibitory control. Nature. 503:521–524.

Purushothaman G, Marion R, Li K, Casagrande VA. 2012. Gating and control of primary visual cortex by pulvinar. Nat Neurosci. 15:905–912.

Reyes A. 2001. Influence of dendritic conductances on the input-output properties of neurons. Annu Rev Neurosci. 24:653–675.

Robinson DL, Petersen SE. 1992. The pulvinar and visual salience. Trends Neurosci. 15:127–132.

Rubio-Garrido P, Perez-de-Manzo F, Porrero C, Galazo MJ, Clasca F. 2009. Thalamic input to distal apical dendrites in neocortical layer 1 is massive and highly convergent. Cereb Cortex. 19:2380–2395.

Shepherd GM, Svoboda K. 2005. Laminar and columnar organization of ascending excitatory projections to layer 2/3 pyramidal neurons in rat barrel cortex. J Neurosci. 25:5670–5679.

Sjostrom PJ, Rancz EA, Roth A, Hausser M. 2008. Dendritic excitability and synaptic plasticity. Physiol Rev. 88:769–840.

Sun YJ, Wu GK, Liu BH, Li P, Zhou M, Xiao Z, Tao HW, Zhang LI. 2010. Fine-tuning of pre-balanced excitation and inhibition during auditory cortical development. Nature. 465:927–931.

Szabadics J, Tamas G, Soltesz I. 2007. Different transmitter transients underlie presynaptic cell type specificity of $GABA_{A,slow}$ and $GABA_{A,fast}$. Proc Natl Acad Sci USA. 104:14831–14836.

Tamas G, Lorincz A, Simon A, Szabadics J. 2003. Identified sources and targets of slow inhibition in the neocortex. Science. 299:1902–1905.

Tamas G, Szabadics J, Somogyi P. 2002. Cell type- and subcellular position-dependent summation of unitary postsynaptic potentials in neocortical neurons. J Neurosci. 22:740–747.

Tomita H, Ohbayashi M, Nakahara K, Hasegawa I, Miyashita Y. 1999. Top-down signal from prefrontal cortex in executive control of memory retrieval. Nature. 401:699–703.

van Boxtel JJ, Tsuchiya N, Koch C. 2010. Consciousness and attention: on sufficiency and necessity. Front Psychol. 1:217.

van Gaal S, Lamme VA. 2012. Unconscious high-level information processing: implication for neurobiological theories of consciousness. The Neuroscientist. 18:287–301.

Waters J, Larkum M, Sakmann B, Helmchen F. 2003. Supralinear Ca2+ influx into dendritic tufts of layer 2/3 neocortical pyramidal neurons in vitro and in vivo. J Neurosci. 23:8558–8567.

Wozny C, Williams SR. 2011. Specificity of synaptic connectivity between layer 1 inhibitory interneurons and layer 2/3 pyramidal neurons in the rat neocortex. Cereb Cortex. 21:1818–1826.

Xu NL, Harnett MT, Williams SR, Huber D, O'Connor DH, Svoboda K, Magee JC. 2012. Nonlinear dendritic integration of sensory and motor input during an active sensing task. Nature. 492:247–251.

Xu X, Callaway EM. 2009. Laminar specificity of functional input to distinct types of inhibitory cortical neurons. J Neurosci. 29:70–85.

Yuen EY, Yan Z. 2009. Dopamine D4 receptors regulate AMPA receptor trafficking and glutamatergic transmission in GABAergic interneurons of prefrontal cortex. J Neurosci. 29:550–562.

Zhang ZW, Deschenes M. 1997. Intracortical axonal projections of lamina VI cells of the primary somatosensory cortex in the rat: a single-cell labeling study. J Neurosci. 17:6365–6379.

Zhu JJ. 2009. Activity level-dependent synapse-specific AMPA receptor trafficking regulates transmission kinetics. J Neurosci. 29:6320–6335.

Zhu JJ. 2000. Maturation of layer 5 neocortical pyramidal neurons: amplifying salient layer 1 and layer 4 inputs by Ca^{2+} action potentials in adult rat tuft dendrites. J Physiol (Lond). 526:571–587.

Zhu JJ, Connors BW. 1999. Intrinsic firing patterns and whisker-evoked synaptic responses of neurons in the rat barrel cortex. J Neurophysiol. 81:1171–1183.

Zhu Y, Stornetta RL, Zhu JJ. 2004. Chandelier cells control excessive cortical excitation: characteristics of whisker-evoked synaptic responses of layer 2/3 nonpyramidal and pyramidal neurons. J Neurosci. 24:5101–5108.

Zhu Y, Zhu JJ. 2004. Rapid arrival and integration of ascending sensory information in layer 1 nonpyramidal neurons and tuft dendrites of layer 5 pyramidal neurons of the neocortex. J Neurosci. 24:1272–1279.